COBEM 2023 27TH INTERNATIONAL CONGRESS OF MECHANICAL ENGENEERING

ABCM Brazilian Society of Mechanical Sciences and Engineering
27th ABCM International Congress of Mechanical Engineering
December 04-08, 2023, Florianópolis-SC, Brazil

COB-2023-1164
NUMERICAL SIMULATION OF A LOCOMOTIVE ENGINE USING DETAILED CHEMICAL KINETICS AS COMBUSTION MODEL AND N-HEPTANE AS DIESEL SURROGATE

Javier Antonio Mendoza Corredor
javier.mendoza@labmci.ufsc.br
Gabriel de Andrade Janene Gonini
gabriel.gonini@labmci.ufsc.br
Milton Keisy Kouketsu
milton.kouketsu@labmci.ufsc.br
Miguel Humberto Barrientos Sandoval
miguel.sandoval@labmci.ufsc.br
Leonel R. Cancino
leonel.cancino@labmci.ufsc.br
Internal Combustion Engines Laboratory - Joinville Technological Center - Federal University of Santa Catarina - LABMCI/CTJ/UFSC. Rua Dona Francisca 8300, Joinville, SC, Brazil, CEP 89219-600
Amir Antônio Martins de Oliveira Jr.
amir.oliveira@ufsc.br
Combustion and Thermal Systems Engineering Laboratory - Technological Center - Federal University of Santa Catarina - LABCET/EMC/CTC/UFSC, Trindade, Florianópolis, SC, CEP 88040-900, Brazil.

Abstract. *Pollution in the world has been the focus of attention in recent years due to its sharp increase. The causes are multiple, and one of them is the emission of pollutants in the rail transport sector. For this, the behavior of the fuel must be known. In the present work, a study of the behavior of a locomotive engine of the VALE company has been carried out. This locomotive has a GE FDL16 model engine. Numerical simulation was performed with AVL-FIRE™ software using detailed chemical kinetics as a combustion model with a kinetics mechanism with 109 species and 543 reactions for combustion predictions, PAH and soot formation validated for the use of n-heptane individually. When comparing the indicated power results with the experimental data, it was observed that the numerical values are consistent and very close. Having a percentage error with the mean value of the indicated power of 2.25%. This shows that the mechanism and the simulation allow reproducing the experimental values. The behavior of the average soot fraction and the average NO fraction for this type of engines was also analyzed.*

Keywords: *Locomotive Engine, AVL-FIRE™ , Detailed chemical kinetics, Compression-Ignition Internal Combustion Engines.*

1. INTRODUCTION

Pollution has garnered significant attention worldwide in recent years due to its substantial increase. There are multiple contributing factors, and one of them is the release of pollutants within the transportation sector, encompassing road, rail, maritime, air, and multimodal transportation (Aminzadegan *et al.*, 2022). Rail transport, in particular, stands out as an ideal means for the large-scale transportation of raw materials or for moving significant numbers of people across extensive distances (Chandra and Agarwal, 2013). This mode of transportation consumes a considerable amount of fuel, leading to a surge in studies focusing on emissions in recent years. It's worth noting that compression ignition engines are commonly utilized in this form of transportation due to their exceptional thermal efficiency and high torque. Nevertheless, these engines generate substantial quantities of pollutant emissions, including NO_X and soot. Consequently, there has been a growing need to implement increasingly stringent emission regulations. Diesel fuel obtained from petroleum is generally used as a fuel. But as a consequence of the environmental problems that are being generated, new alternatives are being sought to reduce these problems. Either by improving the working conditions of the engine to make it more efficient or by changing the fuel for a biofuel. For this purpose, it has been necessary to use computational reactive fluid dynamics (CRFD) simulations, which are capable of representing the behavior of the engine and its fuel in a numerical way. On the other hand, it must be taken into account that the fuel is composed of a large number of species or chemical components that numerically their representation is not feasible in simulations, due to their high computational cost. Therefore, it has been chosen to use diesel surrogates, with a smaller amount of components that are able to represent approximately the behavior of diesel and its combustion process (Westbrook and Dryer, 1981).

Another phenomenon that also plays a very important role in this type of simulations, being one of the three key elements in CRFD along with mesh generation and algorithm development is turbulence. Accurate models have been developed for the first two, but not for turbulence due to its nature (Wilcox *et al.*, 1998). With turbulence eddies appear with a wide range of length and time scales. Being necessary to select a method capable of capturing these effects but that also fits the complexity of the model and the needs of the specific problem studied Versteeg and Malalasekera (2007). On the other hand, *n*-heptane (nC_7H_{16}) as a diesel substitute has been used in different studies (Lu and Law, 2006, 2008; Ranzi *et al.*, 2014; Yoo *et al.*, 2011; Wu *et al.*, 2020; Wang *et al.*, 2015) showing good results.

As already mentioned, it is important to know how Diesel substitutes behave. In this study, a numerical simulation of a four-stroke Diesel locomotive engine was carried out. The simulation will be carried out in AVL-FIRE™ computational fluid dynamics software based on a finite volume approach. Detailed chemical kinetics will be used as the combustion model. A reduced kinetic mechanism (TRF, *n*-heptane, *i*-octane and toluene) with 109 species and 543 reactions capable of predicting the combustion behavior proposed by Wang *et al.* (2015) was used in this work. The results are compared to experimental data in terms of the indicated power obtained from VALE by Henschel Jr. and Cancino (2019). An analysis of the behavior of emissions such as nitrogen oxides and unburned particulate matter is also performed.

2. LITERATURE REVIEW

2.1 Detailed chemical kinetics

The detailed chemical kinetics as a model of combustion is a very important tool in of great importance in the analysis of this phenomenon that allows identifying the chemical behavior during combustion and today has become a valuable material to understand this complex phenomenon (Westbrook and Dryer, 1981). It has been described in kinetics models that allow the prediction of fuel characteristics, the accuracy with which the predictions are made depends on the level of detail of the model (Battin-Leclerc *et al.*, 2013). In chemical kinetics, one can find detailed models of hundreds of species and tens of thousands of reactions to global models with few species and reactions. But since what is sought is accuracy in the numerical representation of a real fuel, one might think that using very large and detailed models is beneficial, but this is not always the case.

The numerical representation of real phenomena is linked and dependent on computational progress at both the software and hardware level, so it is not possible to perform 0-D and even more 3-D simulations using large detailed models due to the large computational consumption required. This motivated the use of smaller, reduced mechanisms that fit the available computational resources but were able to represent the kinetics behavior (Battin-Leclerc *et al.*, 2013). Reduction of the detailed models is performed for a range of pressure, temperature and stoichiometry by applying methods with different approaches. The reduced models are evaluated against the detailed model by comparing the prediction given on parameters such as ignition delay time, laminar flame speed, species concentration, among others (Lu and Law, 2009).

2.2 Kinetics Mechanisms

Kinetics mechanisms are a set of chemical species that represent the fuel, oxidant, intermediates and products, together with the chemical reactions that describe the formation, destruction and interaction of these species. Therefore, they are able to describe what happens at the molecular level, which allows relating macroscopic phenomena to microscopic behavior. There are different types of kinetics models such as global kinetics mechanism that represent the physical-chemical transformation of fuel and oxidant during combustion by means of one or some non-elementary chemical reactions (Merker *et al.*, 2012)). When detailed kinetics mechanisms are not computationally feasible, it is common to use reduced kinetics mechanisms, smaller mechanisms obtained from detailed mechanisms.

In this part skeletal mechanisms are a good choice as they represent a subset of the detailed mechanism. they contain only some of the species and reactions of the original mechanism that are really important for specific conditions (Battin-Leclerc *et al.*, 2013). On the other hand are the semi-detailed mechanisms are those obtained by some methods that seek to further reduce the skeletal mechanisms and further reduce the stiffness, generating smaller mechanisms to be used in complex simulations. In this type of model, some species are grouped together and all their reactions are no longer elementary, but may contain global reactions that represent a group of the elementary reactions. One method used for the development of semi-detailed mechanisms is the Lumping method (Turányi and Tomlin, 2014)

2.3 computational fluid dynamics and turbulence

There are mainly three categories by which the fluid flow can be numerically analyzed: (i) Reynolds-Averaged Navier-Stokes equations (RANS), (ii) Large Eddy Simulation (LES) and, (iii) Direct Numerical Simulation (DNS). Of these categories, the RANS model is the most widely used due to its low computational cost. The RANS model uses the average velocities and properties of the mean flow, so local flow instability cannot be predicted Senecal *et al.* (2012). Simplifications are made in the equations for RANS where the mean flow is analyzed, but additional terms due to transport

properties fluctuations appear and must be solved for. These additional terms can be modeled by using turbulence models. Among the best known are the turbulence models κ - ε, κ - ω, $k-\zeta-f$, the Reynolds stress model, among others. The $k-\zeta-f$ model proposed by Hanjalić *et al.* (2004), where they propose a version of the eddy viscosity model based on the concept of Durbin (1991). It has been widely used for numerical simulations of combustion engines due to its robustness (Merker *et al.*, 2012). The main objective of the model is to improve the numerical stability of the original $\bar{v}^2 - f$ and solving $\zeta = \bar{v}^{-2}/k$ instead of the velocity scale $\bar{v}^2$.

3. METHODOLOGY

The computational analysis was performed with AVL-FIRE™ software in the ESE Diesel module. The strategy chosen was not to include the intake and exhaust cycle because of the lack of data of the valve lift curves, so the simulations would have a shorter calculation time. This means that the study starts from the closing of the intake valve (IVC) to an instant of the opening of the exhaust valve (EVO).

3.1 Engine characteristics

Table 1 presents the main characteristics of a Dash 9-BB40W locomotive engine, the heart of which is a General Electric (GE) diesel engine, model GE FDL16 (Henschel Jr. and Cancino, 2019).

Table 1. Characteristics of a motor General Electric (GE) model GE- FDL16

Parameters	Description	Parameters	Description
Engine configuration	V-16 4-stroke turbocharged	Compression ratio	12.7:1
Valves per cylinder	4	Power	4100 HP
Cylinder diameter [m]	0.2286	Maximum Rotation [rpm]	1050
Crankshaft radius [m]	0.1333	Minimum Rotation [rpm]	333
Connecting rod length [m]	0.5905	Injection Type	Electronic
Stroke [m]	0.2667		

3.2 Initial conditions

The simulation's initial parameters are introduced, encompassing initial conditions defined in terms of pressure, temperature, velocity, and specific turbulence parameters. Additionally, the description encompasses the geometry of both the computational domain employed and the engine injector. Table 2 provides a comprehensive listing of the initial parameters, including engine rotation, pressure, temperature, wall temperatures, energy, turbulent scale length, and other relevant factors.

Table 2. Initial conditions

Parameters	Description	Parameters	Description
Rotation speed [rpm]	996	Swirl [1/min]	2880
Cylinder pressure [kPa]	255	Direction of rotation Z	-1
Temperature [K]	355	Movable wall temperature [K]	570.15
Turbulent kinetic energy [m²/s²]	10	Fixed wall temperature [K]	470.15
Turbulence length scale [m]	0.0045		

3.3 Piston and injector

It was worked with a simplified geometry of forty-five degrees as presented in Table 3. This is done in order to reduce the computational capacity and simulation times. The injector is composed of eight orifices and positioned at an angle of inclination of 160°CA. The values taken for the diameter of the orifices, as shown in Figure 1, were estimated due to lack of data because of the manufacturer.

According to Merker *et al.* (2012) the injector bores for small engines such as passenger car engines have a diameter of 0.12 mm and for compression ignition engines it is approximately 1.5 mm. Therefore, the measurements taken for the injectors to be simulated are within the parameters. Table 4 shows the parameters of the injector geometry and the sketch made in AVL-FIRE™.

Table 3. Geometric piston characteristics.

Piston parameters	
TDC [m] clearance gap	0.01535
Db [m] bowl diameter	0.16180
T[m] bowl Depth	0.02020
Tm [m] bowl Crown height	0.00000
R4 [m] radius	0.01800

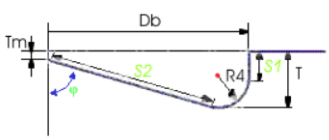

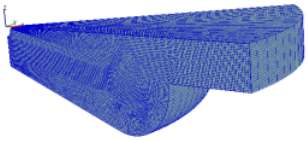

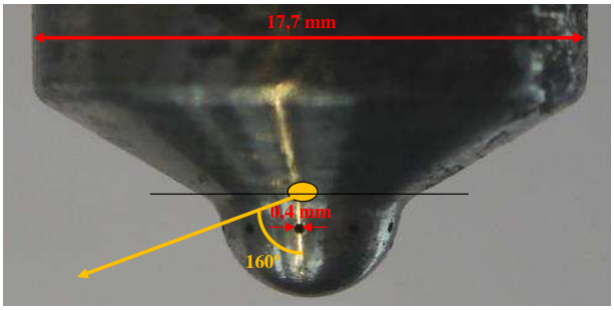

Figure 1. Injector parameters. (Henschel Jr. and Cancino, 2019)

Table 4. Geometric injector characteristics.

Injector geometry parameters	
Number of nozzle holes [-]	8
Injector Spray angle [deg]	160
Nozzle hole outer diameter [m]	0.00040
Injector distance lw [m]	0.00426
Injector tip protrusion lh [m]	0.00380
Radius R1 [m]	0.00236
Radius R2 [m]	0.00130
Distance S1 [m]	0.00102
Distance S2 [m]	0.00088

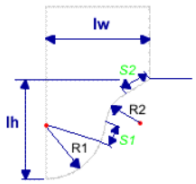

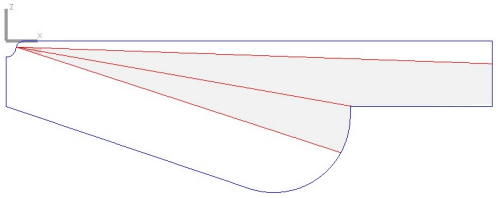

3.4 Kinetics mechanism used in this work

In this work, was used the reduced kinetics mechanism proposed by Wang *et al.* (2015) for reference fuels (TRF *n*-heptane, *i*-octane and toluene) and polycyclic aromatic hydrocarbon (PAH) chemistry with 109 species and 543 reactions proposed for PAH combustion and soot formation predictions was used. The mechanism was validated with various experimental data from a direct injection ignition (DICI) and homogeneously charged compression ignition (HCCI) engine, including laminar flame speed, premixed flame species concentration profiles, and shock tube ignition delay time. The validation conditions for the ignition delay time of *n*-heptane were at initial pressure of 40 bar, $\phi = 1$ and $T = 714$ - 1428 K with experimental data from Herzler *et al.* (2005); Shen *et al.* (2009); Hartmann *et al.* (2011); Fieweger *et al.* (1997). Laminar flame velocities were validated at the conditions of $p = 1.0$ bar, $T = 298$ K and $\phi = 0.6$ - 1.6 using the experimental data of Van Lipzig *et al.* (2011). The species concentration profiles were validated with the experimental data from the literature (Marchal *et al.*, 2009; Bakali *et al.*, 1998; Inal and Senkan, 2002) under the $p = 0.1$ MPa and $\phi = 1.9$ conditions.

3.5 Mesh independence study

Mesh independence was conducted to determine the optimal mesh size for simulation, thereby reducing computational time without compromising result accuracy. For this purpose, the ESE DIESEL mesh generator has been used and the aspect ratio has been varied as a mesh size control parameter. Figure 2(a) shows the different values used and the number of cells for each of the meshes analyzed. The indicated power (kW) was used as an evaluation parameter to determine the most suitable mesh. All these simulations were performed on an 8-core computer with a processing speed of 4.6 GHz and 40 GB of RAM, each simulation had an average duration of 72 hours. Figure 2(b) shows the behavior of the indicated power using different mesh sizes.

When the aspect ratio is decreased, the number of cell sizes increases as shown in Figure 2(a). Six meshes were

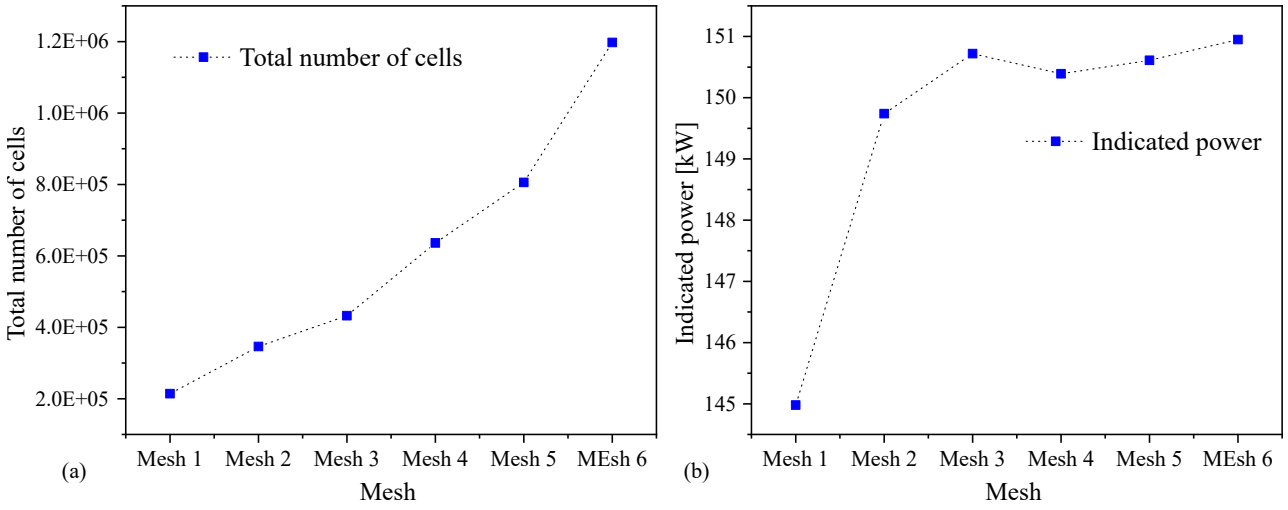

Figure 2. (a) Number of cells per mesh used. (b) Indicated power.

evaluated, each with different sizes, with the finest mesh having a value of 1197416 (mesh 6) cells and the coarsest mesh 214180 (mesh 1). Once the simulations were carried out, it was decided to work with mesh 3 with a size of 432572 because, as shown in Figure 2(b), the value of the indicated power remains relatively constant or with few changes in relation to the finer meshes.

3.6 NO_X and soot formation

For the calculation of NO_X formation, the kinetic mechanism used in this study contains a simplified sub-mechanism of 12 reactions and 4 species, which presents the following reactions:

$$N+NO \rightleftharpoons N2+O \quad (1)$$

$$N+O2 \rightleftharpoons NO+O \quad (2)$$

$$N+OH \rightleftharpoons NO+H \quad (3)$$

$$N2O+O \rightleftharpoons N2+O2 \quad (4)$$

$$N2O+O \rightleftharpoons 2NO \quad (5)$$

$$N2O+H \rightleftharpoons N2+OH \quad (6)$$

$$N2O+OH \rightleftharpoons N2+HO2 \quad (7)$$

$$N2O(+M) \rightleftharpoons N2+O(+M) \quad (8)$$

$$HO2+NO \rightleftharpoons NO2+OH \quad (9)$$

$$NO+O+M \rightleftharpoons NO2+M \quad (10)$$

$$NO2+O \rightleftharpoons NO+O2 \quad (11)$$

$$NO2+H \rightleftharpoons NO+OH \quad (12)$$

The kinetics soot model module incorporated in AVL-FIRE™ was used for soot formation. This uses a global kinetics model reduced from a detailed kinetics mechanism of 850 gas-phase reactions, 186 species among 100 heterogeneous reactions involving four sets of heterogeneous microparticles of different types, whose kinetics parameters have been modified according to the type of fuel used, and for *n*-heptane have been accurately calculated by AVL-FIRE™. Thus, although the kinetics mechanism used as a combustion model contains soot precursor species, the kinetics mechanism of the soot modulus available from AVL-FIRE™generates a total value for the soot produced.

4. RESULT AND DISCUSSION

4.1 Global results

The results obtained numerically will be compared with experimental parameters provided by Vale. These are shown in Table 5. Other parameters will be evaluated by making comparisons between different crankshaft angles, in order to understand the combustion behavior and the formation of pollutants in this type of engines.

Numerically the values obtained for the mean effective pressure and indicated power are shown in Figure 3. The Figure 3(a) allows to visualize the comparison between the experimental and numerical values for the mean effective pressure and the indicated power. It is observed that experimentally there are three values for each parameter, the minimum, the

Table 5. Averaged measured parameters, per piston - Dash 9 BB40W - locomotive VALE (2011)

	Mean Effective Pressure [bar]	Indicate Power [kW]
Average	15.79	154.17
Maximum	16.96	169.27
Minimum	14.13	140.88

maximum and the average value that the mean effective pressure and the indicated power can take. Both parameters are within the maximum limits, i.e., these global parameters were adequately represented by the numerical simulation and the kinetic mechanism. The numerical mean effective pressure was 16.48 bar, i.e., there is a difference of 4.37% in relation to the experimental mean value. Similarly, the numerical indicated power was 150.73 kW, presenting a difference of 2.25% with the experimental average value.

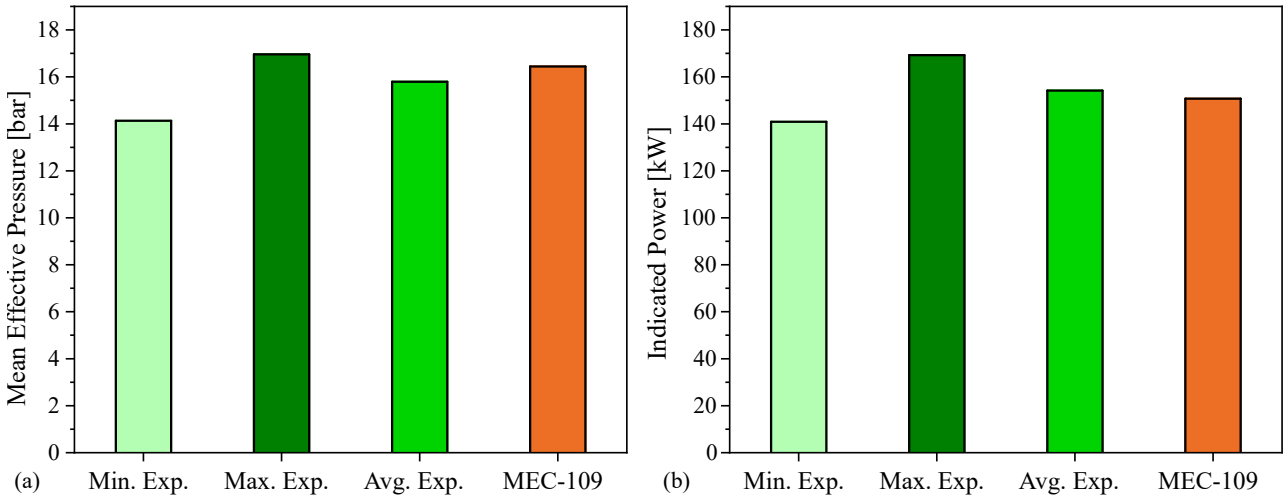

Figure 3. Comparison between the experimental and numerical values for the (a) mean effective pressure and (b) indicated power.

The Figure 4(a) shows the average temperature inside the cylinder as a function of the crank angle. It is observed that from the beginning of the simulation at 560°CA the temperature is increasing until reaching 708°CA where the temperature increase accelerates. Taking into account that fuel injection occurs at 702°CA. Thus, 6°CA after this moment the temperature starts to increase due to fuel ignition. The average temperature takes maximum values around 1596 K between 736°CA and 750°CA. On the other hand, the temperature inside the cylinder can reach 2832 K at 726°CA. The maximum average temperature occurs several degrees later due to the temperature distribution inside the combustion chamber. At the moment combustion starts, the farthest points still remain at lower temperatures, which counteracts the average temperature value. Finally the average temperature at the end of combustion is calculated at 1221.6 K. Figure 4(b) shows the mean total pressure inside the cylinder. This parameter reaches the maximum value around 726°CA - 727°CA with a pressure of 13.1 MPa. It is observed that the value of CA where the maximum temperature inside the cylinder was obtained is equivalent to the point where the maximum Mean Total Pressure was obtained, which was expected.

4.2 Spray

Figure 5 shows the mean Sauter diameter of the spray droplets from 705° CA to 720° CA. Initially the fuel injection is done with a droplet size like the injector nozzle diameter. Subsequently, the spray and wave breakup models calculate the decrease in diameter of the fuel droplets as they penetrate into the cylinder. Thus, the droplets decrease in diameter due to the fuel evaporation process, becoming smaller as shown in Figure 5d. This evaporation process also decreases the energy inside the cylinder. Figure 5 also shows how the spray model numerically represents the droplet size by defined plots.

4.3 Emissions

It is important to know the behavior of the emissions produced during the combustion process. Emissions are products resulting from combustion that are expelled through exhaust gases. Some of these emissions are harmful to human health

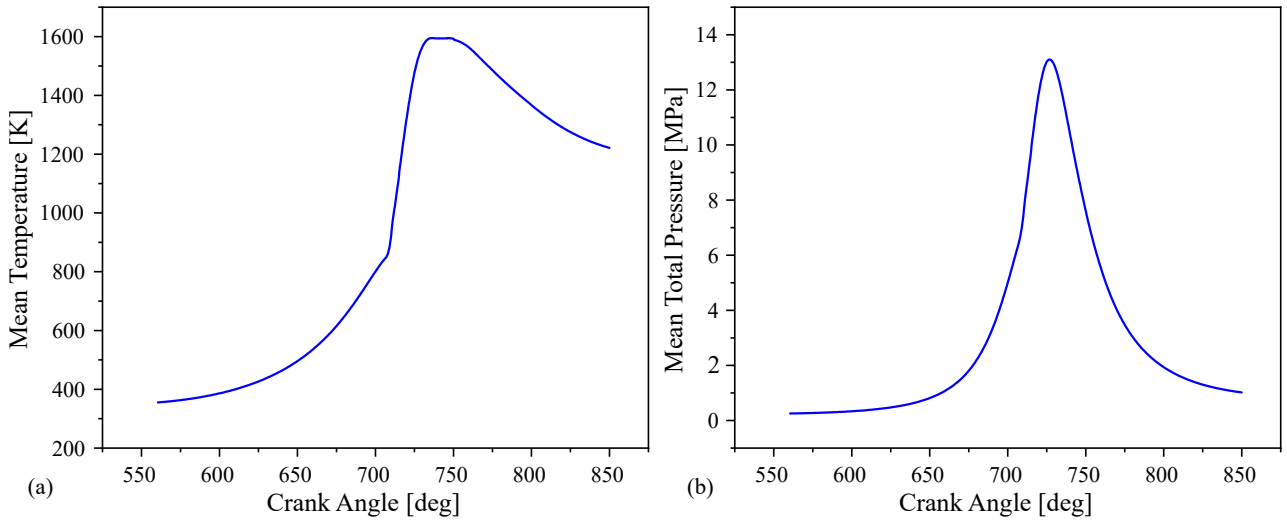

Figure 4. (a) Mean Temperature and (b) Mean Total Pressure.

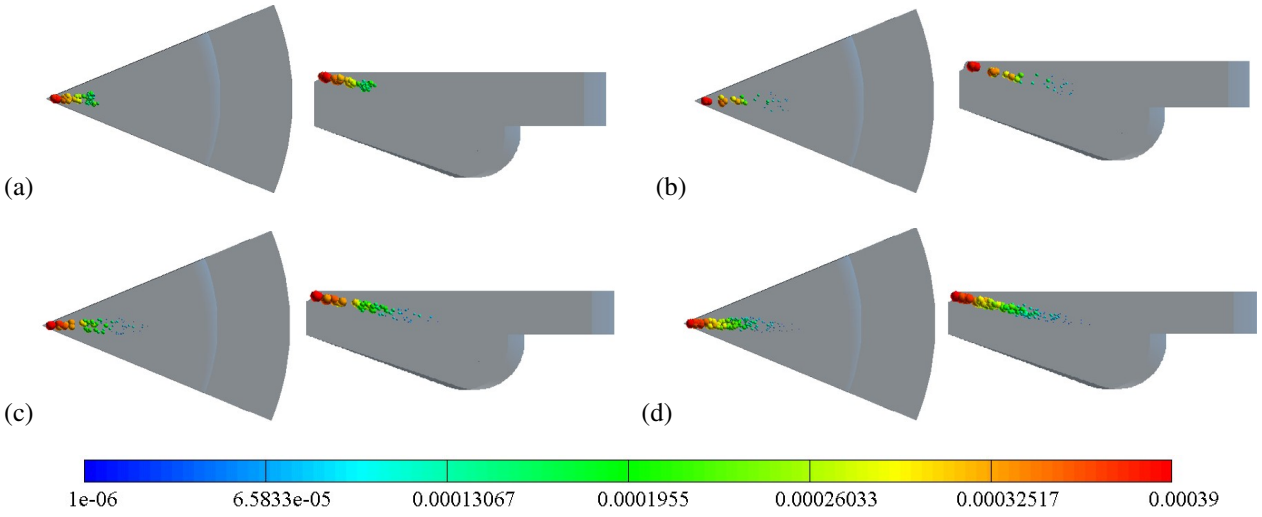

Figure 5. Mean Sauter diameter (d32) [m] behavior for (a) 705°CA, (b) 710°CA, (c) 715°CA and (d) 720°CA.

and contribute to the greenhouse effect, such as carbon monoxide (CO), unburned hydrocarbons (HC), nitrogen oxide (NO_X), unburned particulate matter among others (Merker *et al.*, 2012). It should be noted that the NO emissions is obtained from the main kinetic mechanism used as the combustion model, while the soot emissions is obtained from AVL's internal soot calculation module, which also uses an additional reduced kinetic mechanism for the calculation of this parameter.

Figure 6(a) shows the behavior of the average soot mass fraction. It begins to form 6°CA after injection, reaching a maximum peak near 742°CA with a mean value of approximately 0.000715753. At approximately 717.5°CA there is a small decrease in soot that can be attributed to early oxidation of the first soot particles generated. Then during combustion the amount of soot increases to 742°CA. After the combustion process, the mean soot mass fraction decreases rapidly, oxidizing into smaller hydrocarbons. Figure 6(b) shows the mean NO mass fraction as a function of CA. NO starts to form after 707°CA. At 707°CA a region of the computational domain begins to exhibit temperatures greater than 1800 K. According to (Merker *et al.*, 2012) and (Baumgarten, 2006) above 1800 K is that the NO formation rate starts to become significant. The increase in temperature inside the cylinder therefore generates an increase in NO production, reaching a maximum value of the mean mass fraction around 735°CA, approximately 9°CA after the maximum temperature and pressure inside the cylinder is present. Thus, this rapid NO formation can be attributed to thermal NO from the Zeldovich mechanism (Equations 1-3). Subsequently, some of the generated NO is converted to other species such as NO_2 and N_2O.

Table 7 shows the comparison between the behavior of temperature, soot mass fraction and NO mass fraction at different crankshaft angle (°CA). It is observed that at 4 degrees after injection, NO and soot emissions have not yet formed due to the combustion process not yet taking place. At the angle of 716°CA the temperature increased by about

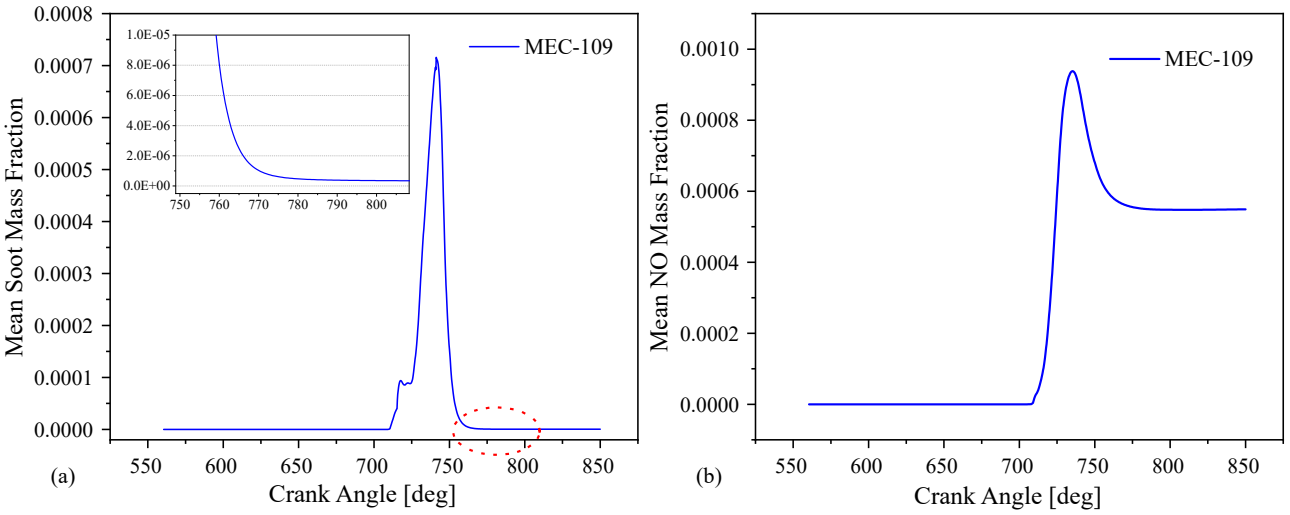

Figure 6. (a) Mean soot mass fraction and (b) NO mass fraction.

1169 K and the formation of small fractions of soot and NO starts. It is usually in the regions where the temperature is higher that NO and soot production begins to occur near the walls where there may be less oxygen. At 735°CA the temperature reaches 1597 K almost at its highest point. In the lower temperature zones there is more soot production. The behavior is the opposite for NO, which has its highest concentrations where the temperature is also highest.

At around 780°CA, near the end of the expansion process, the temperature begins to drop. It is also observed that the cylinder walls are at low temperatures compared to the temperature at the center of the cylinder. For this angle the soot mass fraction is almost zero in all regions of the cylinder, since the combustion process is finished. As for NO, it is observed that its mass fraction has decreased with respect to 735°CA, presenting the highest concentrations after the combustion process. In low temperature zones, NO concentrations are not present.

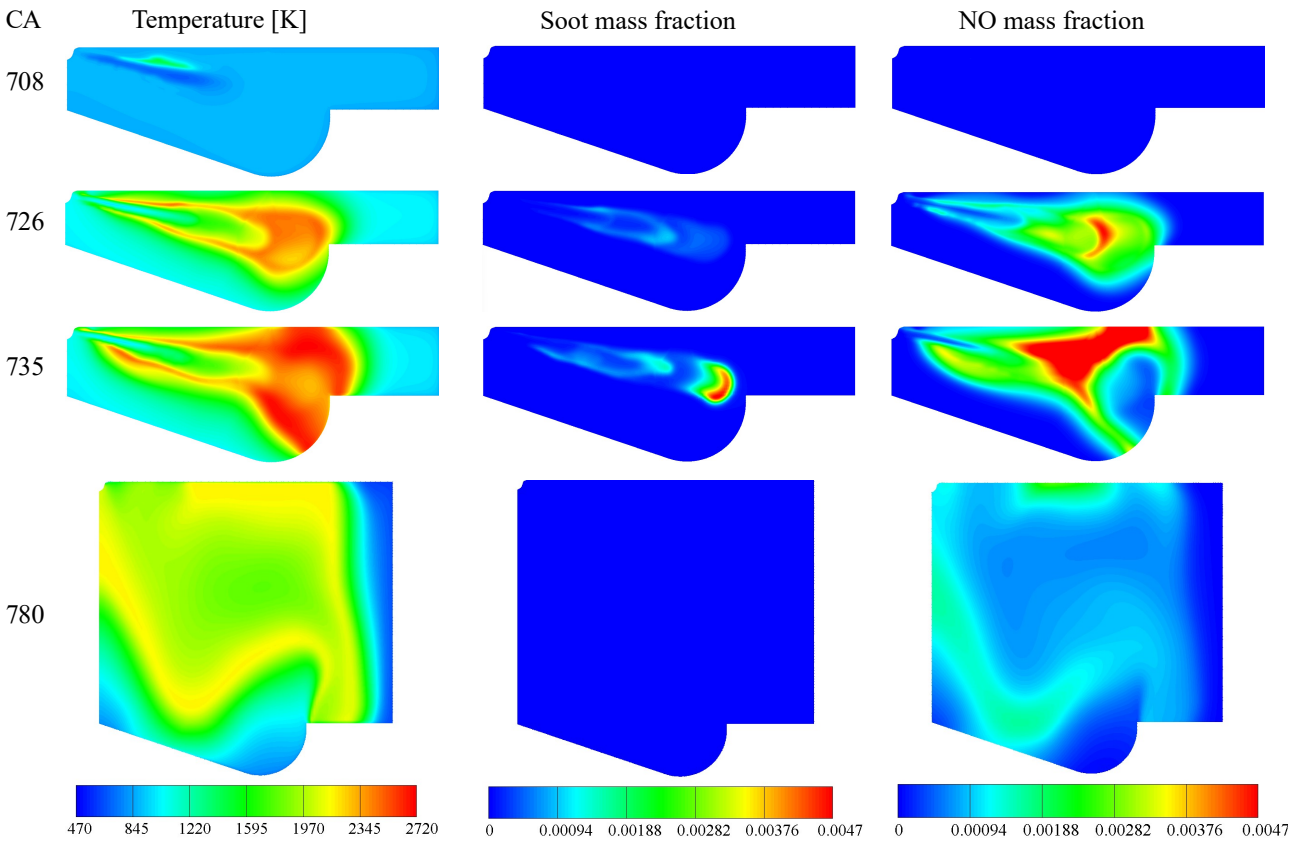

Figure 7. Temperature, soot mass fraction and NO mass Fraction at different crank angle.

The Figure 7 shows the distribution fields for temperature, soot mass fraction and NO mass fraction at different crank angles. These angles were selected as key points for the analysis and visualization of the combustion process. The areas shown correspond to the middle plane of the simulated circular section. As for the temperature, at 708°CA, 6°CA after the start of injection (SOI), a low temperature is observed in the spray region but also a slight increase in the upper part of the spray. Subsequently, at 726°CA, the point where the maximum pressure and temperature is reached, the temperature of the gases increased. Although at this point the maximum temperature is present, in this case it is not located on the plane shown in the Table 7. A few degrees later, combustion is still occurring and therefore, the temperature in the whole space increases.

Likewise, it is observed that the spray region remains at a lower temperature relative to its surroundings where combustion occurs due to the evaporation process of the fuel droplets. After combustion at 780°CA the temperature has decreased significantly, most of the gases are at simulated temperature and the areas of lower temperature corresponds to the cylinder walls due to heat transfer. In relation to the mass fraction of soot and NO, it is observed that only shortly after fuel injection at 708°CA neither of these two pollutants has begun to form. Later at 726°CA when combustion is already occurring, it is observed that NO is generated in greater quantity, as mentioned above due to the high temperatures of the gases. While at this point, since oxygen is still available, the hydrocarbons continue to react. A few degrees later, at 735°CA, the highest concentration of NO is present, while soot has not yet reached its maximum value, which is reached near 742°CA. As the temperature decreases the production rate of NO decreases and it is converted into other compounds, so it is observed that at 780°CA the mole fraction of NO has decreased considerably. The same can be observed with soot, which is observed to continue reacting, reaching very low concentrations at the end of combustion.

5. CONCLUSION

The present work has the vision of incorporating the analysis of high power internal combustion engines, in this case a 4100HP locomotive engine. Using detailed chemical kinetics as a combustion model and verifying the behavior of the Diesel substitutes. The numerical representation of the engine was able to adequately represent the available experimental parameters such as mean effective pressure and indicated power. In relation to the average experimental values, the mean effective pressure presented a difference of only 4.37% and the indicated power a difference of 2.25%. Therefore, it can be said that the kinetic mechanism with 109 species and 543 reactions is a good combustion model for this engine. The pressure and temperature curves of the cylinder were also obtained, showing the combustion process from the increase of pressure and temperature and showing the average values taken by the cylinder in each AC. The average temperature reached a maximum value of 1596 K and the pressure reached 13.1 MPa. The use of chemical kinetics allowed characterizing the formation of pollutants such as soot and NO. It showed that during the moments of higher temperature the NO production increases significantly. The highest amount of soot is produced at 742° CA and then decreases due to the oxidation of these particles due to the available oxygen. Similarly, NO formation occurs up to 735° CA and then decreases somewhat due to the conversion of NO to other species. Since the available experimental parameters such as mean effective pressure and indicated power are reproduced with good accuracy, it is concluded that the model satisfactorily predicts the combustion process using detailed chemical kinetics as a combustion model. Therefore, it is feasible to use the detailed chemical kinetics for further studies to make improvements and optimization of the piston, the type of injection or to analyze other types of fuels such as biodiesel.

6. ACKNOWLEDGEMENTS

The authors acknowledge the AVL AST University Partnership Program (UPP) for the use and support of AVL-AST software. The authors would like to acknowledge to the UFSC Joinville IT (Mr. Kleber Carlos Francisco) team for all support given to the LABMCI/CTJ computer network. The first author acknowledges the financial support granted by the *Coordenação de Aperfeiçoamento de Pessoal de Nível Superior - Brasil* (CAPES) Master's Fellowship Process No. 88887.663145/2022-00.

7. REFERENCES

Aminzadegan, S., Shahriari, M., Mehranfar, F. and Abramović, B., 2022. "Factors affecting the emission of pollutants in different types of transportation: A literature review". *Energy Reports*, Vol. 8, pp. 2508–2529.

Bakali, A.E., Delfau, J.L. and Vovelle, C., 1998. "Experimental study of 1 atmosphere, rich, premixed n-heptane and iso-octane flames". *Combustion science and technology*, Vol. 140, No. 1-6, pp. 69–91.

Battin-Leclerc, F., Simmie, J.M. and Blurock, E., 2013. "Cleaner combustion". *Developing Detailed Chemical Kinetic Models. Series: Green Energy and Technology. Cham: Springer International Publishing AG*.

Baumgarten, C., 2006. *Mixture formation in internal combustion engines*. Springer Science & Business Media.

Chandra, S. and Agarwal, M.M., 2013. *Railway Engineering*. OXFORD UNIVERSITY PRESS, 2nd edition. ISBN 978-0-19-808353-5.

Durbin, P.A., 1991. "Near-wall turbulence closure modeling without "damping functions"". *Theoretical and computational fluid dynamics*, Vol. 3, No. 1, pp. 1–13.

Fieweger, K., Blumenthal, R. and Adomeit, G., 1997. "Self-ignition of si engine model fuels: a shock tube investigation at high pressure". *Combustion and Flame*, Vol. 109, No. 4, pp. 599–619.

Hanjalić, K., Popovac, M. and Hadžiabdić, M., 2004. "A robust near-wall elliptic-relaxation eddy-viscosity turbulence model for cfd". *International Journal of Heat and Fluid Flow*, Vol. 25, No. 6, pp. 1047–1051.

Hartmann, M., Gushterova, I., Fikri, M., Schulz, C., Schießl, R. and Maas, U., 2011. "Auto-ignition of toluene-doped n-heptane and iso-octane/air mixtures: High-pressure shock-tube experiments and kinetics modeling". *Combustion and Flame*, Vol. 158, No. 1, pp. 172–178.

Henschel Jr., J.A. and Cancino, L.R., 2019. "NUMERICAL ANALYSIS OF FUEL SPRAY ANGLE ON THE OPERATING PARAMETERS IN A LOCOMOTIVE DIESEL ENGINE". In *Proceedings of COBEM 2019 - 25th ABCM International Congress of Mechanical Engineering*. ABCM, Uberlândia, Brazil, pp. COB–2019–1642. URL `https://repositorio.ufsc.br/bitstream/handle/123456789/202701/Paper%20COBEM2019%20-%20COB-2019-1642%20-%20John%20Adilson%20Henschel%20Junior.pdf?sequence=1&isAllowed=y`.

Herzler, J., Jerig, L. and Roth, P., 2005. "Shock tube study of the ignition of lean n-heptane/air mixtures at intermediate temperatures and high pressures". *Proceedings of the Combustion Institute*, Vol. 30, No. 1, pp. 1147–1153.

Inal, F. and Senkan, S.M., 2002. "Effects of equivalence ratio on species and soot concentrations in premixed n-heptane flames". *Combustion and flame*, Vol. 131, No. 1-2, pp. 16–28.

Lu, T. and Law, C.K., 2006. "Linear time reduction of large kinetic mechanisms with directed relation graph: n-heptane and iso-octane". *Combustion and flame*, Vol. 144, No. 1-2, pp. 24–36.

Lu, T. and Law, C.K., 2008. "Strategies for mechanism reduction for large hydrocarbons: n-heptane". *Combustion and flame*, Vol. 154, No. 1-2, pp. 153–163.

Lu, T. and Law, C.K., 2009. "Toward accommodating realistic fuel chemistry in large-scale computations". *Progress in Energy and Combustion Science*, Vol. 35, No. 2, pp. 192–215.

Marchal, C., Delfau, J.L., Vovelle, C., Moréac, G., Mounaı, C., Mauss, F. *et al.*, 2009. "Modelling of aromatics and soot formation from large fuel molecules". *Proceedings of the Combustion Institute*, Vol. 32, No. 1, pp. 753–759.

Merker, G.P., Schwarz, C. and Teichmann, R., eds., 2012. *Combustion Engines Development - Mixture Formation, Combustion, Emissions and Simulation*. Springer-Verlag, Berlin Heidelberg. ISBN 978-3-642-02951-6.

Ranzi, E., Frassoldati, A., Stagni, A., Pelucchi, M., Cuoci, A. and Faravelli, T., 2014. "Reduced kinetic schemes of complex reaction systems: fossil and biomass-derived transportation fuels". *International Journal of Chemical Kinetics*, Vol. 46, No. 9, pp. 512–542.

Senecal, P., Pomraning, E., Richards, K. and Som, S., 2012. "Grid-convergent spray models for internal combustion engine cfd simulations". In *Internal Combustion Engine Division Fall Technical Conference*. American Society of Mechanical Engineers, Vol. 55096, pp. 697–710.

Shen, H.P.S., Steinberg, J., Vanderover, J. and Oehlschlaeger, M.A., 2009. "A shock tube study of the ignition of n-heptane, n-decane, n-dodecane, and n-tetradecane at elevated pressures". *Energy & Fuels*, Vol. 23, No. 5, pp. 2482–2489.

Turányi, T. and Tomlin, A.S., 2014. *Analysis of kinetic reaction mechanisms*, Vol. 20. Springer.

VALE, 2011. "Dados da locomotiva dash9-bb40w". *Internal Documentation VALE S.A.-General electric*.

Van Lipzig, J., Nilsson, E., De Goey, L.P. and Konnov, A.A., 2011. "Laminar burning velocities of n-heptane, iso-octane, ethanol and their binary and tertiary mixtures". *Fuel*, Vol. 90, No. 8, pp. 2773–2781.

Versteeg, H.K. and Malalasekera, W., 2007. *An introduction to computational fluid dynamics: the finite volume method*. Pearson Education Ltd, Harlow, England ; New York, 2nd edition. ISBN 978-0-13-127498-3.

Wang, H., Yao, M., Yue, Z., Jia, M. and Reitz, R.D., 2015. "A reduced toluene reference fuel chemical kinetic mechanism for combustion and polycyclic-aromatic hydrocarbon predictions". *Combustion and Flame*, Vol. 162, No. 6, pp. 2390–2404.

Westbrook, C.K. and Dryer, F.L., 1981. "Chemical kinetics and modeling of combustion processes". In *Symposium (International) on Combustion*. Elsevier, Vol. 18, pp. 749–767.

Wilcox, D.C. *et al.*, 1998. *Turbulence modeling for CFD*, Vol. 2. DCW industries La Canada, CA.

Wu, Y., Liu, Y. and Lu, T., 2020. "A linearized error propagation method for skeletal mechanism reduction". *Combustion and Flame*, Vol. 211, pp. 303–311.

Yoo, C.S., Lu, T., Chen, J.H. and Law, C.K., 2011. "Direct numerical simulations of ignition of a lean n-heptane/air mixture with temperature inhomogeneities at constant volume: Parametric study". *Combustion and Flame*, Vol. 158, No. 9, pp. 1727–1741.

8. RESPONSIBILITY NOTICE

The authors are solely responsible for the printed material included in this paper.